Noncanonical P gene mRNA editing in Cedar virus generates a V-like protein that is required for efficient virion production

Henriette Schwotzer[15#], Patricia Schupp[16#], Richard Küchler[17], Dmitry S Ushakov[1], Gang S Pei[2], Sandra Diederich[3], Ilona Ronco[4], Olivier Reynard[4], Branka Horvat[4], Falk Butter[1], Stefan Finke[1*]

[1] Institute of Molecular Virology and Cell Biology, Friedrich-Loeffler-Institut, Greifswald-Insel Riems, Germany

[2] Institute of Immunology, Friedrich-Loeffler-Institut, Greifswald-Insel Riems, Germany

[3] Institute of Novel and Emerging Infectious Diseases, Friedrich-Loeffler-Institut, Greifswald-Insel Riems, Germany

[4] CIRI, Centre International de Recherche en Infectiologie, Inserm, U1111, Université Claude Bernard Lyon 1, CNRS, UMR5308, Ecole Normale Supérieure de Lyon, Lyon, France.

[5] Present address: Institute of Diagnostic Virology, Friedrich-Loeffler-Institut, Greifswald-Insel Riems, Germany

[6] Present address: RNA Biology and Posttranscriptional Regulation, Max Delbrück Center, Berlin, Germany

[7] Present address: Institute for Clinical Chemistry and Laboratory Medicine, Faculty of Medicine, Greifswald

* Corresponding author: Stefan Finke, stefan.finke@fli.de

[#] These authors contributed equally to the study.

Keywords: Henipavirus, Cedar virus, Nipah virus, mRNA editing

Abstract

Highly pathogenic Hendra and Nipah viruses encode accessory P gene products (C, V and W) that antagonize innate immunity and contribute to pathogenicity. Cedar virus (CedV), an apathogenic bat-borne henipavirus, is presumed to lack P gene mRNA editing and therefore is unable to express V and W proteins. Here, we identify CedV peptides originating from a frameshifted P gene open reading frame and demonstrate a previously unrecognized, noncanonical editing event at a homopolymeric adenine tract that introduces single-nucleotide A or G insertion. This mRNA editing produces a V-like protein whose C-terminal domain shares sequence and predicted structural features with those of the henipavirus V protein and displays cytoplasmic and nuclear localization. Recombinant CedV mutants defective in mRNA editing or with a truncated C-terminus were only recoverable by trans-complementation and showed markedly reduced release of infectious virus in cell culture and attenuated replication in mice lacking type I interferon receptor. Our data revise the CedV gene expression models and reveal a noncanonical editing mechanism that supports the production of a V-like protein critical for efficient infectious virus release. These results expand the fundamental concepts of paramyxovirus gene expression and reveal an unexpected, pivotal role for mRNA editing in virus egress, with direct implications for the evaluation of potentially high-consequence paramyxoviruses.

45 **Introduction**

46 Henipaviruses (genus *Henipavirus*, family *Paramyxoviridae*) include the biosafety
47 level 4 (BSL-4) pathogens Nipah virus (NiV) and Hendra virus (HeV). They are
48 enveloped, single-stranded, negative-sense RNA viruses whose genomes encode nine
49 proteins. Three accessory P-gene products (C, V and W) are major pathogenicity
50 factors. The C protein is translated from an alternative downstream open reading
51 frame by leaky scanning, whereas the V and W proteins arise from cotranscriptional
52 mRNA editing that inserts one (in the case of V) or two (in the case of W) guanine
53 nucleotides in the nascent mRNA. This causes a frameshift and generates these
54 distinct C-terminal variants of P (reviewed in (Hantabal et al., 2026)).

55 Cotranscriptional P gene editing is broadly conserved among paramyxoviruses and
56 was first inferred from C-terminally distinct V proteins in simian virus 5 (Thomas et
57 al., 1988). V proteins typically contain a conserved cysteine-rich zinc-finger domain,
58 although truncations without this protein domain have been proposed in some
59 paramyxoviruses, such as Jeilongvirus. Exceptions to V protein expression have
60 indeed been reported in human parainfluenza virus type 1 and Cedar virus (CedV)
61 (Douglas et al., 2021), where the canonical editing motif is absent (Marsh et al.,
62 2012; Matsuoka et al., 1991).

63 In NiV and HeV, the proteins C, V and W antagonize innate immune signaling by
64 interfering with pattern recognition receptor pathways and inhibiting
65 STAT1/2-mediated interferon responses (Ciancanelli et al., 2009; Rodriguez et al.,
66 2003; Rodriguez and Horvath, 2013; Sanchez-Aparicio et al., 2018; Shaw et al.,
67 2004). Additionally, protein W can impair NF-κB signaling through 14-3-3 binding and
68 nuclear sequestration of p65 (Enchery et al., 2021), and it has been linked to the

69 modulation of metabolism and apoptosis (Edwards et al., 2020). These immune
70 evasion strategies are thought to promote sustained replication in
71 immune-competent respiratory epithelia (Muller et al., 2023).

72 CedV is a Pteropus bat-associated henipavirus that is considered apathogenic. CedV
73 was reported to lack the conserved P-gene editing motif (UUUUCCC, genome
74 template orientation) present in NiV and HeV and to harbor a premature stop codon
75 in the putative V open reading frame, suggesting an inability to express functional
76 V. The presumed absence of V and W expression has been proposed to underlie the
77 non-pathogenic phenotype of CedV (Marsh et al., 2012). Furthermore, the lower
78 STAT1 binding capacity of CedV P than that of NiV and HeV (Lieu et al., 2015) and
79 the difference in Ephrin receptor usage between CedV and pathogenic henipaviruses
80 (Haas et al., 2025; Laing et al., 2019) are considered important for the different
81 pathogenic potential of CedV.

82 Despite this, CedV can replicate and disseminate to limited levels in vivo (Chen et
83 al., 2020; Marsh et al., 2012; Schountz et al., 2019) in the presence of an intact type
84 I interferon response. Furthermore, CedV circulates in Pteropus bat colonies,
85 indicating sufficient replication for maintenance in reservoir populations.

86 Here, we use proteomics, targeted sequencing and reverse genetics to identify a
87 previously unrecognized CedV P gene product generated by non-canonical mRNA
88 editing. We show that editing yields a V-like protein that combines the features of
89 the henipavirus V and W proteins and that disruption of this editing event severely
90 impairs the production of infectious viruses both in vitro and in vivo. These findings
91 revise CedV gene annotation and reveal atypical editing mechanisms in henipaviruses
92 that support CedV replication.

93 **Results**

94 **Identification of V-like peptides in the CedV infection proteome.** Proteomic
95 analysis of cell lysates from recombinant CedV (rCedV)-infected SK-N-SH cells at 48
96 hours post-infection (hpi) revealed the expression of all the canonical viral proteins
97 (N, P, M, F, G, L and C) (Fig. 1A). To detect previously unknown proteins, we
98 additionally included an in silico translation of all possible ORFs with at least 20
99 amino acids from the CedV genome during peptide identification. Notably, we found
100 three additional peptides that mapped to the same alternative reading frame within
101 the P gene (genomic nt 3308–3517), corresponding to a stretch of 70 amino acids
102 translated from frame 3 of the P gene (Fig. 1B-E). Two of these peptides showed 44–
103 48% sequence identity to a consensus sequence derived from the C-terminal domains
104 of V proteins from NiV and HeV, suggesting the possibility of a V-like protein with
105 conserved sequence features in CedV (Fig. 1F).

106 **A noncanonical mRNA editing site generates CedV V-like transcripts.** To test
107 whether these peptides arise from mRNA editing, we subjected RT-PCR amplicons
108 from infected human SK-N-SH and HeLa cell lines and bat PATGV cells to
109 next-generation sequencing (NGS). Bioinformatic analysis revealed a hotspot of
110 single-nucleotide insertions at genome position 3312 (P-mRNA position 1299). Unlike
111 canonical paramyxovirus editing, insertions comprising either adenosine or guanosine
112 nucleotides were detected using both oligo(dT) and negative-sense RT primers across
113 different cell types at frequencies of 13 to 20% (Fig. 2A, Table S2). The insertion site
114 comprises a heptameric adenine stretch (TTAAAAAAAGAAA, mRNA orientation) and
115 is located upstream of the canonical editing sites in NiV and HeV. Cloning and Sanger
116 sequencing of independent cDNA clones confirmed the insertions and supported
117 genuine editing rather than sequencing artifacts.

118 **Editing-dependent expression and localization of a CedV V-like protein.** cDNAs
119 from the P gene with single adenosine or guanosine nucleotide insertions at the
120 identified editing site were transfected into BSR T7/5 cells, leading to the synthesis
121 of lower-molecular-weight V-like proteins (Fig. 2B). The A or G nucleotide insertions
122 at the noncanonical site introduce a frameshift and permit translation of a
123 69-amino-acid alternative C-terminus that encompasses the proteomics-identified
124 peptides (Fig. 2C). Compared with NiV P and V, the CedV P protein remained
125 predominantly cytoplasmic in transfected cells, whereas the V-like protein localized
126 to both the cytoplasm and the nucleus (Fig. 2D), suggesting that the alternative
127 C-terminus provides additional trafficking determinants and may combine the
128 properties of the NiV V and W proteins.

129 **Structural and motif predictions reveal hybrid V- and W-like features.** AlphaFold
130 predictions indicated that the CedV V-like protein had a largely disordered
131 architecture with short structured elements and a characteristic two-ß-sheet
132 protrusion in the C-terminal domain (CTD), resembling the NiV V protein CTD (Fig.
133 3A, Fig. S1). While the ß-sheet structure was highly similar between CedV and NiV,
134 CedV mRNA editing led to the formation of a positively charged stretch of five amino
135 acids that is not present in the NiV V protein (Fig. 3B).

136 Linear-motif searches using ELM (Kumar et al., 2024) predicted candidate interaction
137 motifs (including a putative 14-3-3 binding motif) and a bipartite nuclear localization
138 signal created by mRNA editing (Fig. 3CD). These features are consistent with nuclear
139 localization and potential interactions with host factors. Notably, a potential binding
140 site for the kinesin light chain (Lig_KLC1_WD_1) was found in the ß-sheets connecting
141 the loops of the CedV V-like and NiV V proteins. However, neither a bipartite NLS
142 nor a 14-3-3 binding motif was found in the NiV V protein. Instead, these features

143 are part of the NiV W protein, which contains a bipartite NLS at the editing site and
144 two 14-3-3 binding motifs in its CTD (Fig. 3E).

145 These data indicated that the CTD of the CedV V-like protein combines the typical
146 features of both the NiV V protein and the W protein.

147 **Distinct localization of P- and V-like proteins in CedV-infected cells.** Upon
148 transfection, the CedV P protein accumulated in viral cytoplasmic inclusion bodies
149 (IB) in CedV-infected cells, whereas the V-like protein was only marginally enriched
150 in IBs (Fig. 4AB). Instead, the V-like protein remained largely diffuse in the cytoplasm
151 and nucleus, indicating different subcellular distributions of P and V-like protein
152 during infection and supporting a role for the CTD of P in recruitment to IBs. Notably,
153 V-like protein displayed prominent nuclear localization in both infected (Fig. 4AB)
154 and noninfected cells (Fig. 4CD).

155 **CedV V-like protein suppresses type I interferon induction but not interferon**
156 **signaling.** Given that antagonism of innate immune pathways is a hallmark of
157 henipavirus V and W proteins, we compared the ability of the CedV V-like protein to
158 inhibit type I interferon induction and downstream interferon responses with that of
159 known regulators such as the CedV P and the NiV P, V and W proteins. Upon
160 stimulation of RIG-I- or TBK1-dependent signaling, expression of the V-like protein
161 reduced IFN-ß promoter–driven reporter activity. While the antagonistic activity of
162 the CedV-like protein was significantly lower than that of the NiV V protein after
163 RIG-I-mediated stimulation, no significant differences were observed after TBK-1-
164 mediated induction (Fig. 5AB). In contrast, whereas all three tested NiV proteins
165 potently inhibited IFN-induced signaling from 13-fold to 7-fold, CedV P only modestly

166 reduced luciferase reporter activity by 3-fold, and the CedV V-like protein did not
167 significantly suppress the interferon response (Fig. 5C).

168 **Generation of recombinant, editing-defective CedV.** To validate the newly
169 identified editing site, we disrupted the adenine heptamer immediately upstream of
170 the guanine at position 3312 by substituting two of the adenine residues with
171 guanines. In addition, we introduced synonymous marker mutations in the P open
172 reading frame, enabling the detection of potential rapid accumulation of mutations
173 and restoration of a functional editing site following virus rescue (Fig. 6A).

174 Despite multiple rescue attempts, rCedV ΔEdit-I could not be recovered from the
175 cDNA plasmid, although all changes were synonymous for protein P. This rescue
176 failure demonstrates an essential function provided by the V-like protein product
177 that can be expressed only with a functional editing site. We presumed that this
178 failure could be overcome by trans-complementation with ectopically expressed V-
179 like protein.

180 To complement the editing-defective genome, we generated BSR-T7-StrepV cells
181 stably expressing an N-terminally Strep-tagged CedV V-like protein. Expression was
182 confirmed by Western blotting (Fig. 6B). Rescue by trans-complementation on BSR-
183 T7-StrepV cells was successful, as demonstrated by the transfer of infectious virus
184 via culture supernatants to noncomplementing BSR-T7/5 cells.

185 Notably, infection of noncomplementing cells with complemented virus resulted in
186 N and G protein expression and syncytia formation comparable to those of wild-type
187 rCedV, indicating that V-like protein expression is not required for viral gene
188 expression or cell–cell fusion (Fig. 6C). Deep sequencing of the supernatants from

189 two independent rescue experiments confirmed the presence of the engineered
190 rCedV ΔEdit-I sequence.

191 Similarly, rCedV ΔEdit-II (disruption of the A-heptamer only) and rCedV-Stop (a stop
192 codon in the ORF of the V-like C-terminal domain; Fig. 6A) were also only recovered
193 in trans-complementing BSR-T7-StrepV cells, and their sequences were also
194 unchanged, as verified by NGS.

195 Amplicon sequencing of the P gene mRNA from rCedV ΔEdit-I and rCedV ΔEdit-II
196 revealed a complete loss of editing in both mutants (Fig. 7A). In contrast, an editing
197 frequency of 27% in rCedV-Stop confirmed that P gene mRNA editing was maintained
198 in this virus mutant. These results functionally validate the requirement of the
199 homopolymeric seven adenosine tract for CedV P gene mRNA editing. Importantly,
200 the availability of editing-negative mutants without any amino acid changes in the P
201 protein enabled us to specifically assess how P gene editing and expression of the
202 corresponding V-like protein contribute to CedV replication.

203 **The expression of V-like proteins is required for the efficient release of infectious**
204 **virus particles.** Whereas wild-type rCedV infection spread markedly from day 1 to
205 day 2 and produced multiple small secondary syncytia, two independently rescued
206 editing-defective clones (rCedV ΔEdit-Ia and rCedV ΔEdit-Ib) formed almost
207 exclusively large syncytia (Fig. 7B). This pattern is consistent with reduced
208 dissemination via cell-free viruses and a shift toward spread by cell–cell fusion.

209 Despite comparable infections at 22 hpi, as assessed by immunofluorescence (Fig.
210 7B) and by western blot detection of CedV nucleoprotein N (Fig. 7C), the titers of
211 infectious virus released into the supernatant were reduced by 505-fold (ΔEdit-Ia)
212 and 181-fold (ΔEdit-Ib) relative to those of rCedV at 22 hpi (Figure 7D). Although the

213 titers of both mutants increased by 44 hpi, they remained 39-fold (ΔEdit-Ia) and 57-
214 fold (ΔEdit-Ib) lower than the wild-type levels, providing evidence that the loss of P
215 gene editing, and consequently V-like protein expression, impaired the formation
216 and/or release of infectious virions.

217 The negative impact of the editing site mutations in rCedV ΔEdit-I was perfectly
218 confirmed by the rCedV ΔEdit-II mutant lacking synonymous downstream mutations.
219 The infectious virus titers of rCedV ΔEdit-II decreased by 1793- and 177-fold at 20
220 and 44 hpi, respectively, at a lower MOI of 0.01 (Fig. 7E). Limitations in rCedV ΔEdit-
221 II spread and larger syncytia sizes were shown by immunofluorescence imaging (Fig.
222 S2). Notably, imaging analysis of rCedV Stop revealed smaller syncytia at 22 hpi,
223 whereas more efficient spread was indicated by multiple infected cell syncytia at 44
224 hpi. This correlated with infectious virus titers in the cell culture supernatants,
225 which reached wt rCedV levels at 44 hours post-infection (Fig. 7E). As the high
226 infectious virus titers could be a result of either full functionality of the remaining
227 12 V-like amino acids in rCedV stopping or rapid acquisition of mutations that restore
228 full V-like protein expression, the amplicon NGS sequences used for editing
229 frequency calculation (Fig. 7A) were further screened for mutations in the V-like
230 protein coding sequence. Indeed, the TAA stop codon present in rCedV Stop was
231 mutated to CAA or GAA in 11.6% and 1.7% of the reads, respectively, leading to both
232 the loss of the premature stop codon and the translation of a complete V-like protein.
233 Given that wt rCedV comprises an AAA codon at that position, any contamination by
234 authentic CedV virus or sequences could be excluded. Rapid escape mutation of
235 rCedV Stop further demonstrating the major impact of V-like protein expression on
236 CedV replication.

237 **Attenuated replication of V-like protein-deficient CedV in IFNAR-KO mice.** To
238 assess the in vivo replication of the P gene editing–defective virus (rCedV ΔEdit-I),
239 we used an interferon-α/β receptor knockout (IFNAR KO) mouse model, which is
240 permissive for CedV infection (Huaman et al., 2024). Mice were infected
241 intraperitoneally with 3×10^5 $TCID_{50}$ per animal, and viral loads were quantified by
242 measuring CedV N gene RNA levels in selected tissues. At 3 days post-infection (dpi),
243 N-gene RNA levels were reduced by 18- to 68-fold in rCedV ΔEdit-I-infected mice
244 compared with those in rCedV-infected mice when all tested organs were considered.
245 This demonstrated impaired replication of the editing-deficient virus in vivo.
246 Differences between the viruses remained evident at 6 dpi, with 3- to 6-fold lower
247 levels in the lung, kidney and spleen and 40- and 75-fold lower levels in the liver and
248 lymph nodes than in the rCedV (Fig. 8). These results show that CedV P gene editing
249 is necessary for efficient replication in vivo and that less efficient replication is
250 detectable even in the absence of type I interferon signaling.

251 **Discussion**

252 Here, we provide on the example of CedV evidence for noncanonical P gene mRNA
253 editing in henipaviruses and identify a noncanonical alternative P gene product that
254 combines features typically attributed to the V and W proteins of highly pathogenic
255 NiV and HeV and other paramyxoviruses. Because this editing product is generated
256 from an alternative P gene editing site and lacks the cysteine-rich region
257 characteristic of canonical paramyxovirus V proteins, we refer to it as a V-like
258 protein. Strikingly, in contrast to most paramyxovirus V proteins, the CedV V-like
259 protein is required for efficient virus rescue and infectious virus production. P gene
260 editing-defective mutants yielded markedly reduced infectious titers, up to ~1800-
261 fold. Together, these data point to a previously unrecognized contribution of a

262 henipavirus P gene mRNA editing product to late stages of the CedV replication cycle
263 and establish a mechanistic framework for noncanonical paramyxoviral mRNA
264 editing.

265 Canonical paramyxovirus P gene editing is associated with the exclusive insertion of
266 nontemplated guanosine residues at defined editing sequence motifs (e.g., AAAAGGG
267 in NiV/HeV, mRNA orientation). In contrast, CedV editing occurs at a different
268 upstream site (AAAAAAAG; mRNA orientation) and results in site-specific insertion of
269 a single adenosine or guanosine residue. To our knowledge, this combination of
270 editing site sequences and adenosine insertion has not yet been described for
271 paramyxoviruses, expanding the concept of P gene editing beyond the previously
272 established canonical motifs. Consequently, prevailing models of CedV gene
273 expression, particularly the widely held notion that CedV lacks P gene mRNA editing,
274 require revision. Importantly, we demonstrate the existence and functional
275 relevance of this editing event in both infected cell cultures and a susceptible mouse
276 model.

277 The apathogenic phenotype of CedV has been attributed primarily to altered
278 receptor usage and a reduced capacity to antagonize innate immunity. CedV uses
279 ephrin B1 and B2 for entry, whereas NiV and HeV preferentially use ephrin B2 and
280 B3, which are thought to shape tissue tropism and host range (Laing et al., 2019).
281 CedV has been reported to lack canonical P gene editing and therefore to not express
282 the classical V and W proteins implicated in host response antagonism (Marsh et al.,
283 2012). Our findings challenge this concept by demonstrating the expression of an
284 editing-derived V-like protein. However, this V-like protein lacks a cysteine-rich zinc-
285 finger domain (ZnFD) broadly conserved in paramyxoviruses (Ramachandran and
286 Horvath, 2010). Loss of ZnFD could contribute to attenuation, whereas other

287 conserved V and W protein-associated activities may be retained to support
288 replication. In this context, V-like protein expression may be particularly important
289 for time-limited spread in animal models, as previously observed (Schountz et al.,
290 2019), and for maintenance in its natural Pteropus bat reservoir. CedV mutants
291 defective in P mRNA editing replicated less efficiently in vivo, supporting the need
292 for the V-like protein in the infected host.

293 Previous work has shown that ablation of NiV V protein expression converts highly
294 pathogenic NiV into a nonlethal virus in vivo (Satterfield et al., 2015). However,
295 whether the absence of a ZnFD in CedV is functionally equivalent to complete loss
296 of the V protein in NiV and whether this difference accounts for the interferon
297 sensitivity and nonlethal phenotype of CedV. It also remains to be determined
298 whether the contribution of the CedV V-like protein to virus release, described in
299 this study, reflects a broader, conserved function of V proteins in henipaviruses.

300 Mechanistically, the CedV editing site differs from conserved paramyxovirus motifs,
301 which contain U- and C-rich nucleotide stretches on the template and promote
302 exclusive G insertion via polymerase back-slipping (Kolakofsky, 2016). In CedV, A or
303 G insertions at the template sequence (U_7C) imply a different mode of stuttering.
304 Multiple A insertions are hallmarks of poly(A) tail formation by negative-strand RNA
305 virus (NNSV) polymerases through slippage at U-rich transcription stop signals (Ogino
306 and Green, 2019). One possibility is that adenosine insertion at the CedV U-heptamer
307 is driven by polymerase slippage at the CedV U_7C signal, similar to Ebola virus
308 glycoprotein mRNA editing, where adenosine insertion occurs at a U_7G template
309 sequence (Volchkov et al., 1995). G insertions in the CedV P gene mRNA could be
310 facilitated by the downstream template C (U_7C) and the formation of a G:U wobble
311 pair after a one-nucleotide backslip. A template AA dinucleotide upstream of the U-

312 heptamer (AAU_7C) could disfavor extended backsliding by creating A:A mismatches,
313 which are not tolerated at canonical editing sites (Kolakofsky, 2016). This model is
314 also supported by structural constraints of NNSV polymerases, which form relatively
315 short RNA:RNA hybrids with templates 7 to 9 bp in length in paramxoviruses
316 (Hausmann et al., 1999; Peng et al., 2024). The noncanonical U_7C CedV editing site
317 described here fits well in such a hybrid, which may be a structural prerequisite of
318 polymerase slippage at this editing site.

319 Paramyxovirus P proteins are modular, comprising alternating disordered and
320 ordered regions. Structural work on NiV indicates that the P protein multimerization
321 domain forms a tetrameric coiled-coil and engages the polymerase in a distinctive
322 tetrameric arrangement (Yang et al., 2024). In CedV, we found the noncanonical
323 editing site in a region analogous to the canonical NiV and HeV editing position, just
324 upstream of the L-interacting domain. The differences in the intracellular
325 localization in CedV-infected cells and the robust recruitment of P protein to
326 cytoplasmic inclusion bodies versus the cytoplasmic and nuclear patterns of the V-
327 like protein are consistent with different viral or host interaction partners.

328 AlphaFold predictions for CedV V-like and NiV V proteins indicate a conserved C-
329 terminal domain architecture consisting of antiparallel ß-sheets embedded within
330 flexible regions and short helices. Such a ß-sheet-containing CTD is broadly
331 conserved among paramyxovirus V proteins and has been linked to the antagonism
332 of MDA5-mediated signaling and interaction with DDB1 (Li et al., 2006;
333 Ramachandran and Horvath, 2010).

334 Although we did not elucidate the effects of CedV V-like protein on individual innate
335 immune pathways in detail, our data indicate that CedV V-like protein activity is

336 antagonistic to type I interferon induction via RIG-I and TBK1-linked signaling.
337 Whether the different C-termini of CedV V-like and P proteins contribute to
338 antagonistic activities remains to be investigated. Global suppression of the
339 interferon response was not pronounced under our experimental conditions,
340 potentially reflecting the lack of the canonical cysteine-rich zinc-finger domain and
341 suggesting that the CedV V-like protein may have diverged toward functions beyond
342 classical interferon escape.

343 In addition to having protein sequence similarities to those of the NiV and HeV V
344 proteins, the CedV V-like protein presents features reminiscent of those of the NiV
345 W protein. Whereas NiV P and V proteins are predominantly cytoplasmic, W protein
346 is located in the nucleus and modulates host signaling through interactions with 14-
347 3-3 proteins (Edwards et al., 2020; Enchery et al., 2021). In CedV, the V-like protein
348 is localized to both the cytoplasm and the nucleus. Motif analysis predicts a bipartite
349 nuclear localization signal generated within the edited region and candidate linear
350 motifs compatible with 14-3-3 binding in the elongated C-terminus. Together, these
351 observations support a model in which CedV V-like combines a conserved V-type CTD
352 with W-like properties, such as enhanced nuclear targeting and potential 14-3-3
353 binding. Experimental dissection will be required to test these interactions.

354 Genetic analysis further revealed the functional relevance of the V-like protein.
355 Editing-defective viruses (rCedV ΔEdit-I and rCedV ΔEdit-II) and a mutant expressing
356 a CTD-truncated V-like protein (rCedV Stop) demonstrate that V-like expression is
357 critical for efficient infectious virus production. This requirement appears to differ
358 from that of NiV, where the V protein can be ablated and the virus remains
359 recoverable without trans-complementation (Satterfield et al., 2015). Whether the
360 V-like protein encodes a genuinely distinct function or whether related functions

361 have been underappreciated in other henipaviruses remains to be determined.
362 Nevertheless, our data suggest an unanticipated role of the CedV V-like protein in
363 virus assembly and/or release, challenging the prevailing view that P protein variants
364 act solely as immune modulators.

365 Only a few precedents exist for paramyxovirus P gene products that directly promote
366 assembly or budding. With respect to NiV and Sendai virus, their C proteins facilitate
367 virus release via ESCRT interactions, and the V protein of human parainfluenza virus
368 type 2 counteracts tethering to promote virion release (Park et al., 2016; Sakaguchi
369 et al., 2005; Sugahara et al., 2004). In this context, CedV V-like protein may likewise
370 support efficient assembly or budding. Candidate tryptophan-dependent motifs
371 predicted to interact with kinesin light chain 1 (KLC1) and the δ subunit of the COPI
372 coatomer could contribute to transport or trafficking steps relevant to assembly and
373 direct or indirect potential tethering inhibition.

374 Together, our findings reveal that the CedV V-like protein cannot be viewed as a
375 canonical nonstructural interferon antagonist. Instead, the data support a model in
376 which an editing-dependent V-like protein contributes directly to productive virion
377 formation while immune-modulatory properties might have been lost. These results
378 have two implications. First, they suggest that P gene products in henipaviruses may
379 be more functionally integrated into assembly and release than previously
380 appreciated, motivating a renewed analysis of V-family proteins across henipaviruses
381 and related paramyxoviruses. Second, the discovery of noncanonical P gene editing
382 in CedV highlights that genome annotation and risk assessment of emerging
383 paramyxoviruses should explicitly consider alternative editing sites capable of
384 generating protein variants in alternative frames, which may influence viral fitness
385 in reservoir hosts and zoonotic potential.

386 **Materials and Methods**

387 **Cells.** BSR-T7/5 cells were cultivated as described previously (Buchholz et al., 1999).
388 HeLa cells were obtained from the Collection of Cell Lines in Veterinary Medicine
389 (CCLV; FLI Riems) and maintained in RPMI-1640 supplemented with 10% fetal calf
390 serum (FCS). Human neuroblastoma SK-N-SH cells (ATCC HTB-11, (Biedler et al.,
391 1973)) were obtained from LGC (UK) and cultured in ZB28 medium (Ham's F12/IMDM,
392 1:1) supplemented with 10% FCS. The Pteropus giganteus cell line PATGV was
393 described previously (Gaudino et al., 2020).

394 **Viruses and full-length cDNA clones.** Recombinant Cedar virus (rCedV) based on the
395 CedV isolate CG1a genome sequence (GenBank: NC_025351.1) and a red fluorescent
396 reporter–expressing rCedV have been described previously (Lenhard et al., 2025;
397 Schrell et al., 2025). The recombinant viruses rCedV ΔEdit-I, rCedV ΔEdit-II and
398 rCedV-Stop (cDNA clone mutagenesis described below) were rescued in BSR-T7-
399 dStrepV cells by cotransfection of the full-length CedV cDNA plasmid and support
400 plasmids, together with pCAGGS-T7Pol encoding a codon-optimized bacteriophage
401 T7 RNA polymerase (Potratz et al., 2020). Plasmids were transfected at the following
402 amounts per 3.5 cm well: pCAGGS-CedV-N (1.25 µg), pCAGGS-CedV-P (0.8 µg),
403 pCAGGS-CedV-L (0.4 µg), full-length CedV cDNA plasmid (3.0 µg) and pCAGGS-T7Pol
404 (0.5 µg) using Lipofectamine 2000 (Thermo Fisher Scientific) according to the
405 manufacturer's instructions. Viral genomes of all recombinant viruses were
406 confirmed by next-generation sequencing (NGS) of virion RNA extracted from culture
407 supernatants.

408 Working virus stocks of rCedV were generated by infecting ~80% confluent SK-N-SH
409 cells in T75 flasks with 1 ml of BSR-T7/5 rescue supernatant or preexisting virus
410 stocks. Stocks of rCedV ΔEdit-I, rCedV ΔEdit-II and rCedV-Stop were obtained from

411 infected complementing BSR-T7-dStrepV cell cultures. Viral titers (TCID50) were
412 determined by endpoint dilution titration on BSR-T7/5 and SK-N-SH cells.

413 **Construction of mutant full-length CedV cDNA clones.** To generate pCedV-ΔEdit-I,
414 16.6-kb and 3.9-kb fragments were amplified from the CedV full-length cDNA clone
415 using primer pairs 1/2 and 3/4, respectively (Table S1), and assembled by hot fusion
416 cloning (Fu et al., 2014). The adenine heptamer at the noncanonical editing site was
417 disrupted by A-to-G substitutions at CedV genome nucleotide (nt) positions 3307 and
418 3310. In addition, editing-irrelevant marker substitutions (A-to-G and G-to-A) were
419 introduced at nt 3322 and 3342 to facilitate unambiguous identification of the
420 mutant virus, including in the event of reversion at the editing site during
421 amplification on noncomplementing cells.

422 pCedV-ΔEdit-II. pCedV-ΔEdit-II, containing A-to-G substitutions at nt 3307 and 3310,
423 was generated from two PCR fragments (1.6 kb and 3.0 kb) amplified with primer
424 pairs 5/6 and 7/8, respectively (Table S1). The two fragments were joined by fusion
425 PCR using the primers 6/8. The resulting 4.6-kb fragment was assembled together
426 with a 16.6-kb XmaI fragment from the CedV cDNA clone to yield pCedV-ΔEdit-II by
427 hot fusion cloning.

428 pCedV-Stop was generated using a comparable strategy with the 9/10 primer pair.

429 **Sequence verification and data availability.** All plasmid constructs were verified by
430 whole-plasmid sequencing (Eurofins Genomics, Germany). All the mutant virus stocks
431 were sequence-confirmed by next-generation sequencing (NGS) (Eurofins Genomics,
432 Germany). Viral genome sequences are available at Zenodo (DOI
433 10.5281/zenodo.18642052).

434 BSR-T7/5 cells stably expressing CedV Strep-V (BSR-T7-dStrepV) were generated by
435 transfection with pCAGGS-dStrepV-Puro, encoding an N-terminally Strep-tagged
436 CedV V protein and a puromycin resistance cassette. Following puromycin selection,
437 single-cell clones were isolated by limiting dilution in 96-well plates and screened
438 for Strep-V expression by fluorescence microscopy and western blotting using Strep-
439 tag detection.

440 **MS analysis.** Quadruplicate cultures of SK-N-SH cells were grown to 80–90%
441 confluence and infected with rCedV at an MOI of 1. Mock-treated cells served as
442 controls. Infection was carried out for 60 min at 37°C with 5% CO_2. Following
443 incubation, the inoculum was removed, and the cells were maintained in ZB28
444 medium (FLI biobank) until harvest. At 48 hpi, the cells were detached, transferred
445 into 2 ml tubes and precipitated by centrifugation at 300 × g for 5 min (Fresco 21
446 [Thermo Scientific]). The cell pellets were resuspended in 200 µl of RIPA buffer (50
447 mM Tris/HCl (pH 7.5), 1% v/v IGEPAL CA-630, 0.5% v/v sodium deoxycholate, 150 mM
448 NaCl in UP H2O) supplemented with protease inhibitors (1 mM pepstatin A [SERVA
449 Electrophoresis GmbH], 1 mg/ml leupeptin [SERVA Electrophoresis GmbH], 100 mM
450 PMSF [SERVA Electrophoresis GmbH]) and 0.5 M EDTA. The lysates were incubated on
451 ice for 30 min, followed by vortexing and centrifugation at 10.000 × g (Fresco 21
452 [Thermo Scientific]) for 10 min at 4°C. The supernatants were transferred into new
453 tubes, and glycerol (Carl Roth) was added to a final concentration of 10% (v/v). The
454 protein concentration was determined by a BCA protein assay (Fisher Scientific) and
455 measured on a GloMax Discover Microplate Reader (Promega). For proteomic
456 analysis, 20 µg of total protein per sample was resuspended in 1× elution buffer (1×
457 LDS [Thermo Fisher Scientific] supplemented with 100 mM DTT [Sigma–Aldrich]) and
458 incubated at 70 °C for 10 min at 1400 rpm in a Thermomixer (Eppendorf). The

459 samples were subsequently processed for mass spectrometry using a previously
460 described in-gel digestion protocol (Scherer et al., 2020). A total of 400 ng of peptide
461 per sample was separated on an Aurora Ultimate™ 25×75 C18 UHPLC column
462 (ionopticks) using a nanoElute HPLC system (Bruker). Separation was conducted with
463 a 100-min gradient at a constant flow rate of 300 nl*min^{-1} with increasing ACN
464 concentration from 2% MS-grade ACN/0.1% formic acid (0–2 min) to 17% (2–67 min),
465 27% (67–88 min), 95% (88–97 min) and 4% (97–100 min). The column was mounted on
466 a timsTOF HT mass spectrometer (Bruker) operated in standard PASEF data-
467 dependent acquisition mode with a cycle time of 1.1 sec. Raw data were processed
468 with MaxQuant (version 2.4.2.0) and searched against the SwissProt (42,338 entries)
469 and Trembl (54,436 entries) (UP000005640, v20200117) *Homo sapiens* databases and
470 all CedV proteins (JQ001776.1). To identify potential unknown viral open reading
471 frames, the nucleotide sequences of all viral proteins were translated into all
472 possible reading frames using the six-frame translation tool in MaxQuant (version
473 2.4.2.0), with a minimal AA length of 20. Downstream data analysis was performed
474 using R-studio (version [2023.06.1]).

475 **Antibodies, sera and imaging.** Polyclonal serum against CedV N was generated at
476 the FLI by immunization of rabbits with a purified CedV N antigen from *Spodoptera*
477 *frugiperda* (Sf9) insect cells infected with a recombinant baculovirus encoding the
478 CedV N carrying an N-terminal histidine tag. CedV G–specific mouse monoclonal
479 antibodies were generated at the FLI by immunization of mice with purified CedV G
480 antigen produced in *Leishmania tarentolae*, as previously described by HeV G
481 (Fischer et al., 2016). A Strep-tag–specific polyclonal rabbit antibody (Thermo Fisher
482 Scientific, PA5-119772) diluted in PBS was used at 1:1,000 for immunofluorescence
483 and 1:2,500 for western blotting. For immunofluorescence microscopy, Alexa Fluor

484 488– and Alexa Fluor 568–conjugated secondary antibodies (Thermo Fisher Scientific)
485 were used at dilutions of 1:1,000 in PBS. For Western blotting, IRDye 680RD anti-
486 mouse and IRDye 800CW anti-rabbit secondary antibodies were used (Li-COR
487 Biosciences, Germany). Nuclear DNA was counterstained with Hoechst 33342 (1 µg
488 ml−1 in PBS). Fluorescence microscopy images were acquired with a Leica THUNDER
489 imager DMi8 with 20×/0.40 dry HC PL FLUOTAR L objectives and LAS X software and
490 with a Leica Stellaris 8 confocal laser scanning microscope with a 63 x/1.40 oil
491 immersion HCX PL APO objective and LAS AF software (Leica Microsystems,
492 Germany). Fluorescent Western blots were imaged with an Odyssey CLx infrared
493 imaging system (Li-COR Biosciences). The images were processed with the Fiji
494 (ImageJ 1.53t) software package (Schindelin et al., 2012).

495 **RNA preparation, reverse transcription, PCR and amplicon sequencing.** Total RNA
496 was isolated from HeLa and SK-N-SH cells at 48 h post infection (hpi) using an RNeasy
497 Mini Kit (Qiagen, 74104) according to the manufacturer's instructions. First-strand
498 cDNA synthesis was performed with a RevertAid First Strand cDNA Synthesis Kit
499 (Thermo Fisher Scientific, K1622) using either oligo(dT) primers or the P gene–
500 specific negative-sense primer 11 (Table S1).

501 A 1,278-bp fragment spanning the CedV P gene was amplified from cDNA using
502 primers 11 and 12 (Table S1) and Phusion Hot Start Flex DNA Polymerase (New
503 England Biolabs, M0535L). The PCR conditions were as follows: 94°C for 2 min; 29
504 cycles of 94°C for 15 s, 58°C for 15 s and 72°C for 1 min; 72°C for 10 min; and a hold
505 at 4°C. Amplicons were purified using the QIAquick Nucleotide Removal Kit (Qiagen,
506 28306) and subjected to Illumina-based amplicon sequencing (Eurofins Genomics).
507 For PATGV cells, total RNA was extracted using the NucleoSpin RNA Mini kit
508 (Macherey-Nagel). The P gene amplicon was generated as described above with P-

509 specific primers and the SuperScript IV One-Step RT–PCR System (Thermo Fisher
510 Scientific).

511 Sequencing data were processed in Geneious Prime using paired-end read assembly,
512 trimming with BBDuk, read normalization (target coverage 40; minimum depth 6)
513 and mapping to the CedV P coding sequence. Nucleotide insertions were called by
514 SNP/variant analysis using a 3% frequency threshold and a minimum coverage of 10
515 reads.

516 **Cloning of P gene sequences into expression plasmids.** A 2.2-kb fragment
517 encompassing the CedV P gene coding region was amplified from the total RNA of
518 rCedV-infected SK-N-SH cells by reverse transcription and PCR amplification using
519 negative-sense primer 13, followed by PCR with primer 13/14 (Table S1). The
520 amplicon was inserted into a pCAGGS-based mammalian expression vector (Niwa et
521 al., 1991) carrying an N-terminal double Strep-tag (dStrep) by assembly with the 4.8-
522 kb NotI/XhoI backbone fragment. Plasmids encoding the unedited P open reading
523 frame were designated pCAGGS-dStrepCedV-P. Plasmids containing a single-
524 nucleotide insertion at the P gene editing site were designated pCAGGS-dStrepCedV-
525 V. To generate pCAGGS-dStrepV-Puro, a pCAGGS derivative containing an EMCV
526 internal ribosome entry site (IRES) and a puromycin resistance cassette downstream
527 of the EcoRI site was linearized with EcoRI. A 1.6-kb insert was amplified from
528 pCAGGS-dStrepCedV-V using the primers 15/16 and assembled into the linearized
529 backbone by hot fusion cloning.

530 **Protein structure analysis.** Protein structure predictions were generated with
531 ColabFold version 1.5.5 (Jumper et al., 2021; Mirdita et al., 2022) using its default
532 parameters and the integrated Amber module for relaxation and energy minimization
533 (Eastman et al., 2017). A total of five models per protein were predicted and ranked

534 according to their mean pLDDT. Structural evaluation and visualization were
535 performed with ChimeraX (Pettersen et al., 2021).

536 **IFNß promoter and interferon-stimulated response element (ISRE) luciferase**
537 **reporter assays.** For human IFNß promoter induction assays, HEK293T cells were
538 transfected with an IFN-ß promoter firefly luciferase reporter plasmid (Promega,
539 USA) together with other plasmids as indicated in the corresponding experiments
540 using PEI 25 kDa transfection reagent (Polyplus, France). At 24 h post transfection,
541 the cell lysates were mixed with the substrate D-luciferin. For the ISRE luciferase
542 assay, HEK293T cells were transfected with the ISRE reporter plasmid (#90402;
543 Addgene, USA) as indicated. At 24 h post transfection, the cells were treated with
544 universal IFN-I (800 U/ml) overnight, and the cell lysates were mixed with the
545 substrate D-luciferin. Luminescence was measured with a TECAN Spark® 3
546 microplate reader (Tecan Group Ltd., Switzerland).

547 **Infection of mice.** All work involving live CedV infections was performed under BSL-
548 2 conditions at PBES, Lyon, France. IFNAR-/- mice were inoculated intraperitoneally
549 (IP) with 3.10^5 TCID50 of rCedV or rCedV ΔEdit-I (volume inoculated of 200 µl) under
550 inhalational anesthesia with isoflurane (isoflurane: ISOFLUTEK 1000 mg/g;
551 Laboratorios Karizoo S.A.; anesthesia station: MiniHUB-V3; TEM SEGA, France). After
552 CedV IP infection, the mice were monitored daily, and selected organs (lungs,
553 kidneys, spleen, livers and mesenteric lymph nodes) were collected at the
554 designated time points (3 and 6 days post-infection). The animal groups were as
555 follows: rCedV-wt_d3: 4 animals; rCedV-wt_d6: 4 animals; rCedV-DelEdit_d3: 4
556 animals; and rCedV-DelEdit_d6: 5 animals.

557 **Sample collection and** RT-qPCR. The mice were euthanized by cervical dislocation
558 under isoflurane. The lungs, spleen, liver, kidneys and mesenteric lymph nodes were
559 harvested. The tissues were snap-frozen at −80°C for molecular analyses. For RNA
560 extraction, ≤30 mg of tissue was homogenized in RA1 buffer (NucleoSpin RNA,
561 Macherey-Nagel) containing ß-mercaptoethanol using a MagNA Lyser and
562 centrifuged, and the supernatant was mixed with 70% ethanol before column-based
563 purification according to the manufacturer's instructions. RNA was used directly for
564 viral detection or DNase treatment. RT-qPCR was performed using the Luna Universal
565 One-Step RT-qPCR Kit on a StepOnePlus™ system. Viral loads are expressed as
566 copies/mg of tissue. CedV-N was detected using the specific primers 17 and 18.

567 **References**

568 Biedler, J.L., Helson, L., Spengler, B.A., 1973. Morphology and growth,
569 tumorigenicity, and cytogenetics of human neuroblastoma cells in
570 continuous culture. Cancer Res 33, 2643-2652.

571 Buchholz, U.J., Finke, S., Conzelmann, K.K., 1999. Generation of bovine
572 respiratory syncytial virus (BRSV) from cDNA: BRSV NS2 is not essential for
573 virus replication in tissue culture, and the human RSV leader region acts as a
574 functional BRSV genome promoter. J Virol 73, 251-259.

575 Chen, M., Tachedjian, M., Marsh, G.A., Cui, J., Wang, L.F., 2020. Distinct Cell
576 Transcriptomic Landscapes Upon Henipavirus Infections. Front Microbiol 11,
577 986.

578 Ciancanelli, M.J., Volchkova, V.A., Shaw, M.L., Volchkov, V.E., Basler, C.F., 2009.
579 Nipah virus sequesters inactive STAT1 in the nucleus via a P gene-encoded
580 mechanism. J Virol 83, 7828-7841.

581 Douglas, J., Drummond, A.J., Kingston, R.L., 2021. Evolutionary history of
582 cotranscriptional editing in the paramyxoviral phosphoprotein gene. Virus
583 Evol 7, veab028.

584 Eastman, P., Swails, J., Chodera, J.D., McGibbon, R.T., Zhao, Y., Beauchamp,
585 K.A., Wang, L.P., Simmonett, A.C., Harrigan, M.P., Stern, C.D., Wiewiora,
586 R.P., Brooks, B.R., Pande, V.S., 2017. OpenMM 7: Rapid development of high
587 performance algorithms for molecular dynamics. PLoS Comput Biol 13,
588 e1005659.

589 Edwards, M.R., Hoad, M., Tsimbalyuk, S., Menicucci, A.R., Messaoudi, I., Forwood,
590 J.K., Basler, C.F., 2020. Henipavirus W Proteins Interact with 14-3-3 To
591 Modulate Host Gene Expression. J Virol 94.

592 Enchery, F., Dumont, C., Iampietro, M., Pelissier, R., Aurine, N., Bloyet, L.M.,
593 Carbonnelle, C., Mathieu, C., Journo, C., Gerlier, D., Horvat, B., 2021.
594 Nipah virus W protein harnesses nuclear 14-3-3 to inhibit NF-kappaB-induced
595 proinflammatory response. Commun Biol 4, 1292.

596 Fischer, K., dos Reis, V.P., Finke, S., Sauerhering, L., Stroh, E., Karger, A.,
597 Maisner, A., Groschup, M.H., Diederich, S., Balkema-Buschmann, A., 2016.
598 Expression, characterisation and antigenicity of a truncated Hendra virus
599 attachment protein expressed in the protozoan host Leishmania tarentolae.
600 J Virol Methods 228, 48-54.

601 Fu, C., Donovan, W.P., Shikapwashya-Hasser, O., Ye, X., Cole, R.H., 2014. Hot
602 Fusion: an efficient method to clone multiple DNA fragments as well as
603 inverted repeats without ligase. PLoS One 9, e115318.

604 Gaudino, M., Aurine, N., Dumont, C., Fouret, J., Ferren, M., Mathieu, C., Reynard,
605 O., Volchkov, V.E., Legras-Lachuer, C., Georges-Courbot, M.C., Horvat, B.,
606 2020. High Pathogenicity of Nipah Virus from Pteropus lylei Fruit Bats,
607 Cambodia. Emerg Infect Dis 26, 104-113.

608 Haas, G.D., Escaffre, O., Reis, R.A., Juelich, T.L., Smith, J.K., Zhang, L.,
609 Kalveram, B.K., Guzmán-Solís, A.A., Vyshenska, D., Klain, W., Greninger,
610 A.L., Freiberg, A.N., Lee, B., 2025. De novo recovery of Ghana
611 virus, an African bat Henipavirus, reveals differential tropism and
612 attenuated pathogenicity compared to Nipah virus. bioRxiv,
613 2025.2010.2008.679836.

614 Hantabal, J., Salguero, F.J., Carroll, M.W., 2026. Current knowledge on the host-
615 pathogen interactions of henipaviruses and novel platforms to enable further
616 characterisation. EBioMedicine 123, 106110.

617 Hausmann, S., Garcin, D., Delenda, C., Kolakofsky, D., 1999. The versatility of
618 paramyxovirus RNA polymerase stuttering. J Virol 73, 5568-5576.

619 Huaman, C., Clouse, C., Rader, M., Yan, L., Bai, S., Gunn, B.M., Amaya, M., Laing,
620 E.D., Broder, C.C., Schaefer, B.C., 2024. An in vivo BSL-2 model for
621 henipavirus infection based on bioluminescence imaging of recombinant
622 Cedar virus replication in mice. Front Chem Biol 3.

623 Jumper, J., Evans, R., Pritzel, A., Green, T., Figurnov, M., Ronneberger, O.,
624 Tunyasuvunakool, K., Bates, R., Zidek, A., Potapenko, A., Bridgland, A.,
625 Meyer, C., Kohl, S.A.A., Ballard, A.J., Cowie, A., Romera-Paredes, B.,
626 Nikolov, S., Jain, R., Adler, J., Back, T., Petersen, S., Reiman, D., Clancy,
627 E., Zielinski, M., Steinegger, M., Pacholska, M., Berghammer, T.,
628 Bodenstein, S., Silver, D., Vinyals, O., Senior, A.W., Kavukcuoglu, K., Kohli,
629 P., Hassabis, D., 2021. Highly accurate protein structure prediction with
630 AlphaFold. Nature 596, 583-589.

631 Kolakofsky, D., 2016. Paramyxovirus RNA synthesis, mRNA editing, and genome
632 hexamer phase: A review. Virology 498, 94-98.

633 Kumar, M., Michael, S., Alvarado-Valverde, J., Zeke, A., Lazar, T., Glavina, J.,
634 Nagy-Kanta, E., Donagh, J.M., Kalman, Z.E., Pascarelli, S., Palopoli, N.,
635 Dobson, L., Suarez, C.F., Van Roey, K., Krystkowiak, I., Griffin, J.E., Nagpal,
636 A., Bhardwaj, R., Diella, F., Meszaros, B., Dean, K., Davey, N.E., Pancsa, R.,
637 Chemes, L.B., Gibson, T.J., 2024. ELM-the Eukaryotic Linear Motif resource-
638 2024 update. Nucleic Acids Res 52, D442-D455.

639 Laing, E.D., Navaratnarajah, C.K., Cheliout Da Silva, S., Petzing, S.R., Xu, Y.,
640 Sterling, S.L., Marsh, G.A., Wang, L.F., Amaya, M., Nikolov, D.B., Cattaneo,
641 R., Broder, C.C., Xu, K., 2019. Structural and functional analyses reveal
642 promiscuous and species specific use of ephrin receptors by Cedar virus.
643 Proc Natl Acad Sci U S A 116, 20707-20715.

644 Lenhard, L., Muller, M., Diederich, S., Loerzer, L., Friedrichs, V., Kollner, B.,
645 Finke, S., Dorhoi, A., Pei, G., 2025. Ephrin B1 and B2 Mediate Cedar Virus
646 Entry into Egyptian Fruit Bat Cells. Viruses 17.

647 Li, T., Chen, X., Garbutt, K.C., Zhou, P., Zheng, N., 2006. Structure of DDB1 in
648 complex with a paramyxovirus V protein: viral hijack of a propeller cluster in
649 ubiquitin ligase. Cell 124, 105-117.

650 Lieu, K.G., Marsh, G.A., Wang, L.F., Netter, H.J., 2015. The non-pathogenic
651 Henipavirus Cedar paramyxovirus phosphoprotein has a compromised ability
652 to target STAT1 and STAT2. Antiviral Res 124, 69-76.

653 Marsh, G.A., de Jong, C., Barr, J.A., Tachedjian, M., Smith, C., Middleton, D., Yu,
654 M., Todd, S., Foord, A.J., Haring, V., Payne, J., Robinson, R., Broz, I.,
655 Crameri, G., Field, H.E., Wang, L.F., 2012. Cedar virus: a novel Henipavirus
656 isolated from Australian bats. PLoS Pathog 8, e1002836.

657 Matsuoka, Y., Curran, J., Pelet, T., Kolakofsky, D., Ray, R., Compans, R.W., 1991.
658 The P gene of human parainfluenza virus type 1 encodes P and C proteins
659 but not a cysteine-rich V protein. J Virol 65, 3406-3410.

660 Mirdita, M., Schutze, K., Moriwaki, Y., Heo, L., Ovchinnikov, S., Steinegger, M.,
661 2022. ColabFold: making protein folding accessible to all. Nat Methods 19,
662 679-682.

663 Muller, M., Fischer, K., Woehnke, E., Zaeck, L.M., Pronnecke, C., Knittler, M.R.,
664 Karger, A., Diederich, S., Finke, S., 2023. Analysis of Nipah Virus Replication
665 and Host Proteome Response Patterns in Differentiated Porcine Airway
666 Epithelial Cells Cultured at the Air-Liquid Interface. Viruses 15.

667 Niwa, H., Yamamura, K., Miyazaki, J., 1991. Efficient selection for high-expression
668 transfectants with a novel eukaryotic vector. Gene 108, 193-199.

669 Ogino, T., Green, T.J., 2019. RNA Synthesis and Capping by Non-segmented
670 Negative Strand RNA Viral Polymerases: Lessons From a Prototypic Virus.
671 Front Microbiol 10, 1490.

672 Park, A., Yun, T., Vigant, F., Pernet, O., Won, S.T., Dawes, B.E., Bartkowski, W.,
673 Freiberg, A.N., Lee, B., 2016. Nipah Virus C Protein Recruits Tsg101 to
674 Promote the Efficient Release of Virus in an ESCRT-Dependent Pathway.
675 PLoS Pathog 12, e1005659.

676 Peng, Q., Dong, Y., Jia, M., Liu, Q., Bi, Y., Qi, J., Shi, Y., 2024. Cryo-EM structure
677 of Nipah virus L-P polymerase complex. Nat Commun 15, 10524.

678 Pettersen, E.F., Goddard, T.D., Huang, C.C., Meng, E.C., Couch, G.S., Croll, T.I.,
679 Morris, J.H., Ferrin, T.E., 2021. UCSF ChimeraX: Structure visualization for
680 researchers, educators, and developers. Protein Sci 30, 70-82.

681 Potratz, M., Zaeck, L., Christen, M., Te Kamp, V., Klein, A., Nolden, T., Freuling,
682 C.M., Muller, T., Finke, S., 2020. Astrocyte Infection during Rabies
683 Encephalitis Depends on the Virus Strain and Infection Route as
684 Demonstrated by Novel Quantitative 3D Analysis of Cell Tropism. Cells 9.

685 Ramachandran, A., Horvath, C.M., 2010. Dissociation of paramyxovirus interferon
686 evasion activities: universal and virus-specific requirements for conserved V
687 protein amino acids in MDA5 interference. J Virol 84, 11152-11163.

688 Rodriguez, J.J., Wang, L.F., Horvath, C.M., 2003. Hendra virus V protein inhibits
689 interferon signaling by preventing STAT1 and STAT2 nuclear accumulation. J
690 Virol 77, 11842-11845.

691 Rodriguez, K.R., Horvath, C.M., 2013. Amino acid requirements for MDA5 and LGP2
692 recognition by paramyxovirus V proteins: a single arginine distinguishes MDA5
693 from RIG-I. J Virol 87, 2974-2978.

694 Sakaguchi, T., Kato, A., Sugahara, F., Shimazu, Y., Inoue, M., Kiyotani, K., Nagai,
695 Y., Yoshida, T., 2005. AIP1/Alix is a binding partner of Sendai virus C protein
696 and facilitates virus budding. Journal of Virology 79, 8933-8941.

697 Sanchez-Aparicio, M.T., Feinman, L.J., Garcia-Sastre, A., Shaw, M.L., 2018.
698 Paramyxovirus V Proteins Interact with the RIG-I/TRIM25 Regulatory Complex
699 and Inhibit RIG-I Signaling. J Virol 92.

700 Satterfield, B.A., Cross, R.W., Fenton, K.A., Agans, K.N., Basler, C.F., Geisbert,
701 T.W., Mire, C.E., 2015. The immunomodulating V and W proteins of Nipah
702 virus determine disease course. Nat Commun 6, 7483.

703 Scherer, M., Levin, M., Butter, F., Scheibe, M., 2020. Quantitative Proteomics to
704 Identify Nuclear RNA-Binding Proteins of Malat1. Int J Mol Sci 21.

705 Schindelin, J., Arganda-Carreras, I., Frise, E., Kaynig, V., Longair, M., Pietzsch, T.,
706 Preibisch, S., Rueden, C., Saalfeld, S., Schmid, B., Tinevez, J.Y., White,
707 D.J., Hartenstein, V., Eliceiri, K., Tomancak, P., Cardona, A., 2012. Fiji: an
708 open-source platform for biological-image analysis. Nat Methods 9, 676-682.

709 Schountz, T., Campbell, C., Wagner, K., Rovnak, J., Martellaro, C., DeBuysscher,
710 B.L., Feldmann, H., Prescott, J., 2019. Differential Innate Immune

711 Responses Elicited by Nipah Virus and Cedar Virus Correlate with Disparate In
712 Vivo Pathogenesis in Hamsters. Viruses 11.

713 Schrell, L., Fuchs, H.L., Dickmanns, A., Scheibner, D., Olejnik, J., Hume, A.J.,
714 Reineking, W., Stork, T., Muller, M., Graaf-Rau, A., Diederich, S., Finke, S.,
715 Baumgartner, W., Muhlberger, E., Balkema-Buschmann, A., Dobbelstein, M.,
716 2025. Inhibitors of dihydroorotate dehydrogenase synergize with the broad
717 antiviral activity of 4'-fluorouridine. Antiviral Res 233, 106046.

718 Shaw, M.L., Garcia-Sastre, A., Palese, P., Basler, C.F., 2004. Nipah virus V and W
719 proteins have a common STAT1-binding domain yet inhibit STAT1 activation
720 from the cytoplasmic and nuclear compartments, respectively. J Virol 78,
721 5633-5641.

722 Sugahara, F., Uchiyama, T., Watanabe, H., Shimazu, Y., Kuwayama, M., Fujii, Y.,
723 Kiyotani, K., Adachi, A., Kohno, N., Yoshida, T., Sakaguchi, T., 2004.
724 Paramyxovirus Sendai virus-like particle formation by expression of multiple
725 viral proteins and acceleration of its release by C protein. Virology 325, 1-
726 10.

727 Thomas, S.M., Lamb, R.A., Paterson, R.G., 1988. Two mRNAs that differ by two
728 nontemplated nucleotides encode the amino coterminal proteins P and V of
729 the paramyxovirus SV5. Cell 54, 891-902.

730 Volchkov, V.E., Becker, S., Volchkova, V.A., Ternovoj, V.A., Kotov, A.N., Netesov,
731 S.V., Klenk, H.D., 1995. GP mRNA of Ebola virus is edited by the Ebola virus
732 polymerase and by T7 and vaccinia virus polymerases. Virology 214, 421-430.

733 Yang, G., Wang, D., Liu, B., 2024. Structure of the Nipah virus polymerase
734 phosphoprotein complex. Nat Commun 15, 8673.

735

Acknowledgments

We are grateful to Angela Hillner, Institute of Molecular Virology and Cell Biology, for perfect technical assistance. We thank Sven Sander and Sven Reiche for support with the production of monoclonal antibodies. This work was supported by intramural funding to Stefan Finke. We acknowledge the contributions of the CELPHEDIA Infrastructure (http://www.celphedia.eu/), especially the center AniRA in Lyon. We acknowledge the contribution of SFR Biosciences (Universite Claude Bernard Lyon 1, CNRS UAR3444, Inserm US8, ENS de Lyon) and notably the PBES facility. Ilona Ronco was funded for her Ph. D by the Direction Générale de l'Armement (DGA) and the Agence Innovation Défense (AID).

Author contributions

Stefan Finke, Falk Butter, Branka Horvat and Olivier Reynard designed the research. Research was performed by Henriette Schwotzer, Patricia Schupp, Ilona Ronco, and Gang Pei. Richard Küchler performed Alphafold predictions. Dmitry Ushakov, Henriette Schwotzer, Patricia Schupp, and Falk Butter performed the data analysis. Sandra Diederich generated CedV-specific antibodies. Stefan Finke, Henriette Schwotzer and Patricia Schupp wrote the manuscript. All the authors were involved in proofreading and finalizing the manuscript.

Competing Interests

The authors declare that they have no competing interests.

Data and Materials availability

The authors declare that the data are available in the publication, supplementary materials or at the public depository Zenodo (DOI 10.5281/zenodo.18642052).

759 **Figure Legends**

760 **Figure 1: Identification of alternative P gene reading frame peptides in CedV-**
761 **infected cells and their similarity to those of the henipavirus V protein. (A)**
762 Volcano plot showing upregulated proteins in CedV-infected SK-N-SH cells, as
763 determined by label-free quantitative proteomics (n = 4). Enriched proteins (p value
764 < 0.05 (Welch's t test) and fold change (FC) > 2) are marked in blue. Canonical CedV
765 proteins are highlighted in orange, and the CedV P gene alternative frame is
766 highlighted in red. **(B-D)** Representative MS/MS spectra of the three detected
767 peptides with b and y ions. **(E)**. Schematic drawing of the CedV genome with
768 annotated ORFs and the nucleotide sequence around amino acid position 408 of the
769 P gene with the editing site of NiV and HeV. The localization of the three identified
770 peptides within the 69-amino acid stretch of ORF frame 3 is illustrated. **(F)** Consensus
771 sequence generated of the C-terminal domains of the HeV and NiV V proteins on the
772 basis of 57 gene bank sequences (list of sequences at DOI 10.5281/zenodo.18642052).
773 Peptides p1 and p3 mapped to the consensus sequence, whereas p2 did not show
774 similarity to the consensus sequence. Positions with amino acid identity between the
775 consensus sequence and CedV peptide are marked by bold letters.

776 **Figure 2: Positions of CedV mRNA editing, expression and localization of V-like**
777 **proteins. (A)** Proportion of editing events detected in P gene mRNA amplified by
778 either negative (-) sense or oligo-dT reverse transcription (RT) primers from isolated
779 total RNA from CedV-infected SK-N-SH, HeLa, and PATGV cells. Frequencies of A and
780 G insertions [1 =100%] are indicated by green and blue, respectively. **(B)** Western
781 blot of Strep-tagged P variants in BSR-T7/5 cells expressed from the cloned and
782 mutated P gene cDNA sequences at 20 h post transfection. **(C)** Position 3312
783 insertions (red letters) result in a frameshift and expression of a 69-aa alternative V-

784 like CTD (C-terminal domain, blue letters) comprising the identified peptides 1, 2
785 and 3. **(D)** Intracellular localization of expressed Strep-tagged CedV and NiV P protein
786 variants expressed from their cDNA sequences in BSR-T7/5 cells at 20 h post
787 transfection. Ctrl: BSR-T7/5 cells transfected with the empty vector. The nuclei are
788 marked by a white star.

789 **Figure 3: Structural predictions of the CedV V-like and NiV V proteins. (A)**
790 Alphafold prediction of the CedV V-like and NiV-V structures with CTDs labeled in
791 orange and magenta, respectively. **(B)** Ribbon diagrams of CedV V-like and NiV V CTD
792 overlays. RMSD: Root mean square deviation. Right: space filling representation of
793 the CTDs with an applied electrostatic potential surface. Blue: positive charge, red:
794 negative charge. The ß-sheets connecting loops are indicated. **(C)** Localization of the
795 linear interaction motif obtained from ELM predictions for the CedV V-like and NiV V
796 proteins. **(D)** Predicted bipartite nuclear localization signal (NLS) in the CedV V-like
797 protein, which consists of positively charged amino acids upstream of the editing site
798 and its CTD. **(E)** A positively charged bipartite NLS in the NiV W protein is generated
799 by editing. Two predicted interaction motifs for binding of 14-3-3 proteins are noted
800 for the NiV W protein CTD.

801 **Figure 4: Immunofluorescence detection of Strep-tagged CedV P and V-like**
802 **proteins in rCedV-infected and noninfected cells. (A, B)** Two hours after infection
803 (MOI = 0.1), BSR-T7/5 cells were transfected with plasmids encoding N-terminally
804 Strep-tagged CedV P or V-like proteins. Immunofluorescence staining was performed
805 16 h posttransfection with antibodies specific for the Streptag (green) and CedV N
806 proteins (magenta). **(C, D)** Plasmid-derived CedV P and V-like protein localization in
807 noninfected cells. Blue: Hoechst 33324 stain.

808 **Figure 5: CedV V-like protein inhibits IFN induction but fails to inhibit the**
809 **interferon response.** Inhibition of IFN-ß promoter induction in HEK293T cells
810 expressing the indicated NiV and CedV P gene products together with human RIG-I
811 **(A)** and TBK1 **(B)** at 24 h post transfection. **(C)** Interferon-stimulated response
812 element (ISRE) activation was measured in HEK293T cells expressing the indicated
813 NiV and CedV P gene products upon universal IFN-I stimulation for 16–24 h. Data are
814 presented as the mean ± SEM. Statistical analysis was performed using one-way
815 ANOVA, followed by the Dunnett multiple comparison test. P values are indicated as
816 ns ($p > 0.05$), * ($p \leq 0.05$), and ** ($p \leq 0.01$). *** ($p \leq 0.001$) and **** ($p \leq 0.0001$). Each
817 dot represents one independent experiment.

818 **Figure 6: Rescue of mRNA editing-defective rCedV ΔEdit in cells complementing**
819 **V-like protein. (A)** Disruption of the heptameric adenine stretch of the CedV editing
820 site, as indicated by blue lowercase letters. With respect to rCedV-ΔEdit-I,
821 downstream guanine and adenine stretches were altered by synonymous mutations
822 in the P protein. For rCedV ΔEdit-II, only the homopolymeric adenine tract of the
823 editing site was modified. For rCedV-Stop, generation of a stop codon in the V-like
824 ORF at the marked position in blue resulted in a truncated V-like protein with only
825 12 amino acids C-terminally of the editing site. **(B)** Western blot detection of the
826 Strep-tagged CedV V-like protein in expression plasmid-transfected BSR-T7/5 cells
827 and in the cell line stably expressing the V-like protein BSR-T7-StrepV. *: presumably
828 truncated V-like protein. **(C)** Infection of noncomplementing BSR-T7/5 cells with
829 rCedV ΔEdit-I after virus rescue in V-like complementing BSR-T7-StrepV cells and
830 rCedV at 22 hpi (magenta: N protein, green: G protein, blue: Hoechst 33324 stain).

831 **Figure 7: CedV P mRNA editing is required for efficient release of infectious**
832 **viruses. (A)** Frequencies of adenosine and guanosine at editing nucleotide position

833 3312 for rCedV, rCedV ΔEdit-I, rCedV ΔEdit-II, and rCedV Stop. Frequencies of A and
834 G insertions [1 =100%] are indicated by green and blue, respectively **(B)** Detection of
835 rCedV ΔEdit-I and rCedV in BSR-T7/5 cells at 22 and 44 hpi by immunofluorescence
836 with two independently rescued rCedV ΔEdit-I (Ia and Ib) viruses (green: G, blue:
837 Hoechst 33324 stain). **(C)** Western blot detection of the CedV N protein (magenta)
838 to confirm comparable infection and virus protein expression after infection at an
839 MOI of 0.1. **(D)** Infectious virus titers in the supernatants of infected cells at 22 and
840 44 hpi. The titers of rCedV were set to 100% for each experimental replicate (n=3).
841 **(E)** Infectious virus titers in the supernatants of rCedV , rCedV ΔEdit-II- and rCedV
842 Stop (MOI 0.01)-infected cells at 20 and 44 hpi. The titers of rCedV were set to 100%
843 for each experimental replicate (n=3) **(F)** Frequencies of the mutations in the
844 inserted stop codon of the rCedV Stop at 20 h post transfection. The data (in D–F)
845 are presented as the mean ± SEM. Statistical analysis was performed using one-way
846 ANOVA, followed by Dunnett's multiple comparisons test. Statistical significance is
847 indicated as **** ($p < 0.0001$). Each dot indicates one independent experiment.

848 **Figure 8. Attenuated replication of V-like-deficient CedV in IFNAR-KO mice.** CedV
849 N gene RNA levels in different organs after intraperitoneal infection at 3×10^5 $TCID_{50}$
850 per mouse. The data are presented as the mean ± SD. Statistical analyses were
851 performed using GraphPad Prism. Differences between groups were analyzed using
852 the Mann–Whitney U test. Statistical significance is indicated as * ($p < 0.05$); ns = not
853 significant ($p \geq 0.05$). Each group consisted of 4–5 animals.

854

855 **Fig. 1**

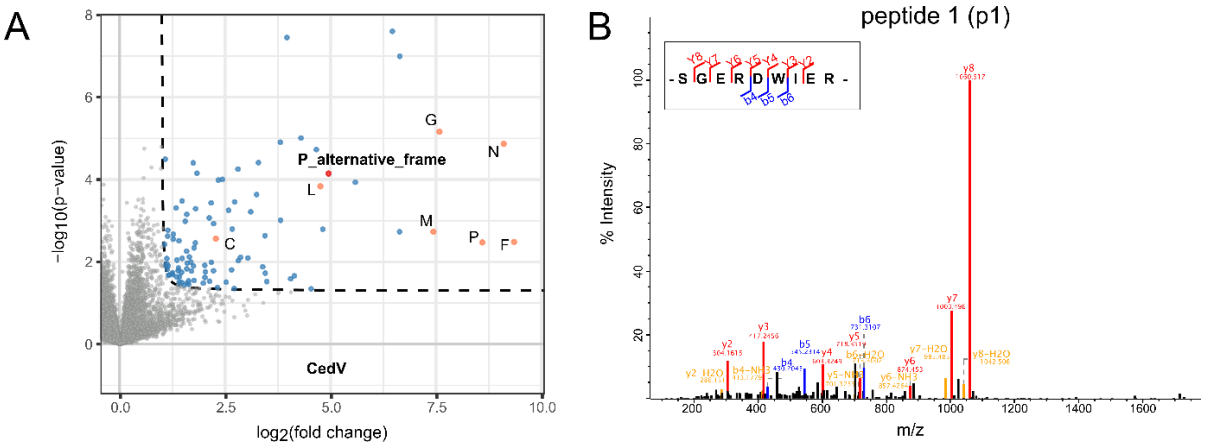
A
-log10(p-value)
log2(fold change)
P_alternative_frame
G
N
L
M
P
F
C
CedV
B
peptide 1 (p1)
-S G E R D W I E R -
% Intensity
m/z

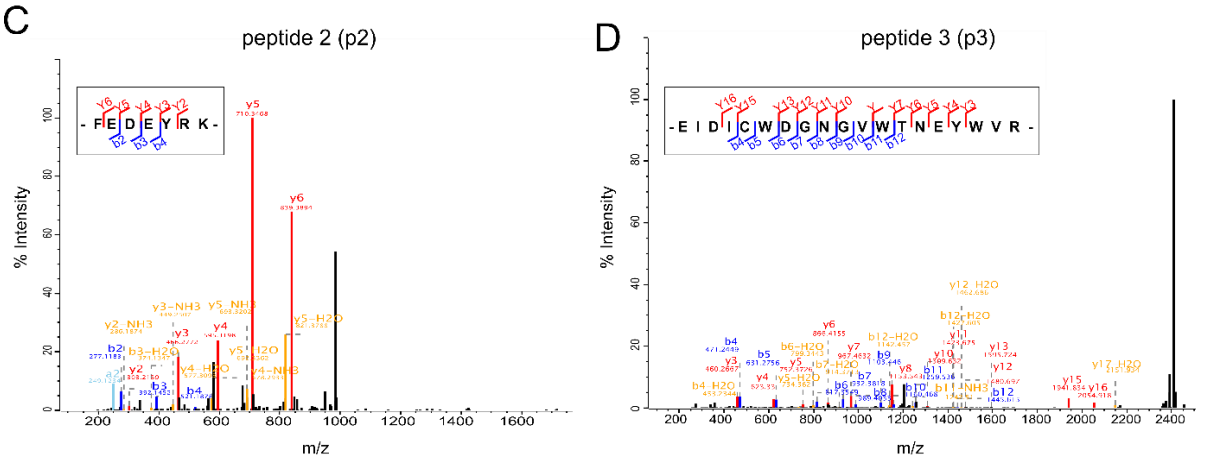
C
peptide 2 (p2)
-F E D E Y R K -
% Intensity
m/z
D
peptide 3 (p3)
-E I D I C W D G N G V W T N E Y W V R -
% Intensity
m/z

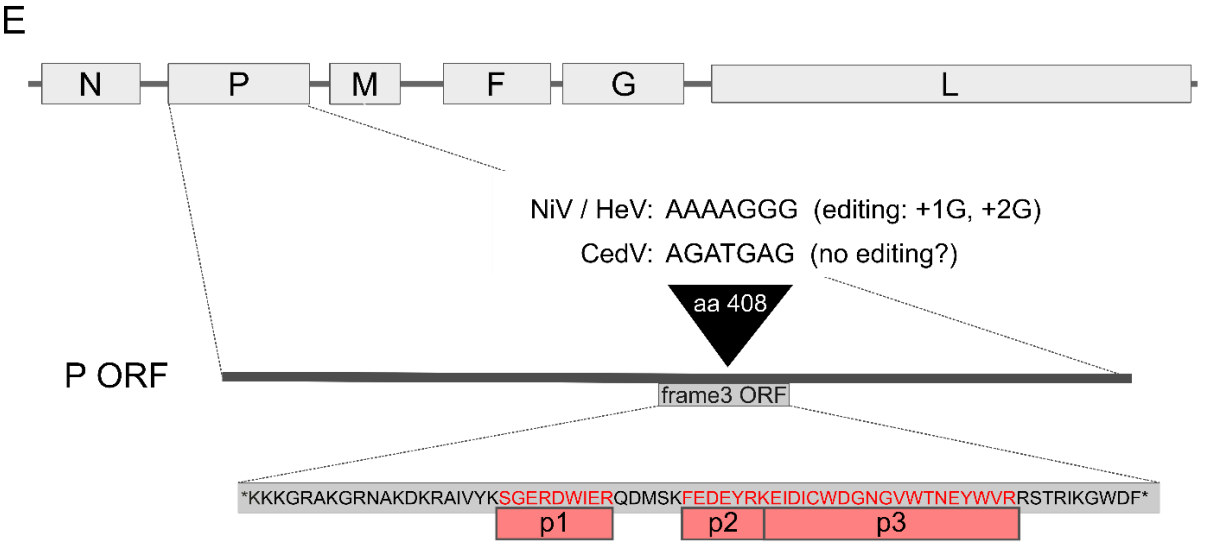
E
N
P
M
F
G
L
NiV / HeV: AAAAGGG (editing: +1G, +2G)
CedV: AGATGAG (no editing?)
aa 408
P ORF
frame3 ORF
KKKGRAKGRNAKDKRAIVYKSGERDWIERQDMSKFEDEYRKEIDICWDGNGVWTNEYWVRRSTRIKGWDF
p1
p2
p3

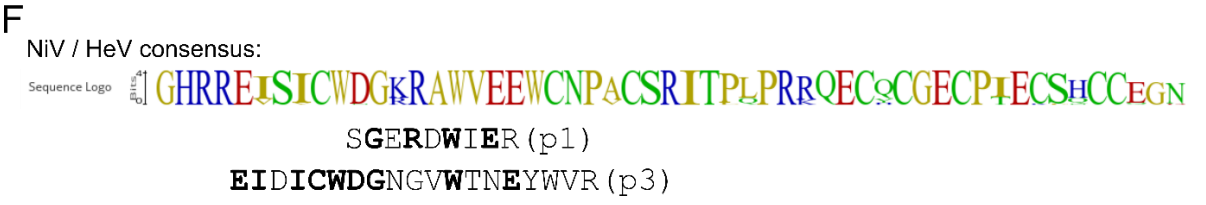
F
NiV / HeV consensus:
Sequence Logo
SGERDWIER(p1)
EIDICWDGNGVWTNEYWVR(p3)

856

857 **Fig. 2**

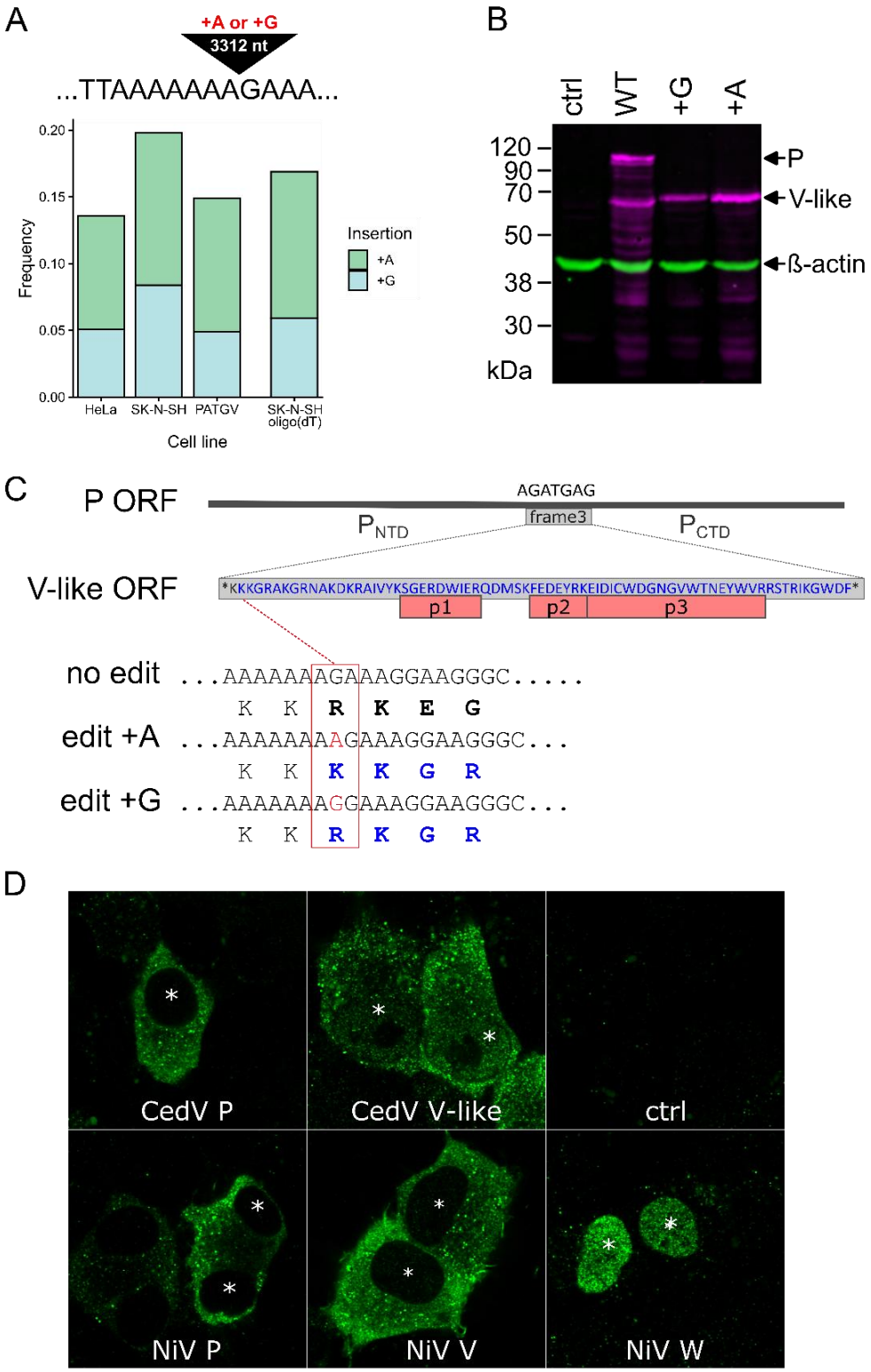
A
+A or +G
3312 nt
...TTAAAAAAAGAAA...
Frequency
0.20
0.15
0.10
0.05
0.00
HeLa
SK-N-SH
PATGV
SK-N-SH oligo(dT)
Cell line
Insertion
+A
+G
B
ctrl
WT
+G
+A
120
90
70
50
38
30
kDa
P
V-like
ß-actin
C
P ORF
AGATGAG
frame3
P NTD
P CTD
V-like ORF
KKKGRAKGRNAKDKRAIVYKSGERDWIERQDMSKFEDEYRKEIDICWDGNGVWTNEYWVRRSTRIKGWDF
p1
p2
p3
no edit ...AAAAAAAGAAAGGAAGGGC.....
K K R K E G
edit +A ...AAAAAAAAGAAAGGAAGGGC...
K K K K G R
edit +G ...AAAAAAAGGAAAGGAAGGGC...
K K R K G R
D
CedV P
CedV V-like
ctrl
NiV P
NiV V
NiV W

858

859 **Fig. 3**

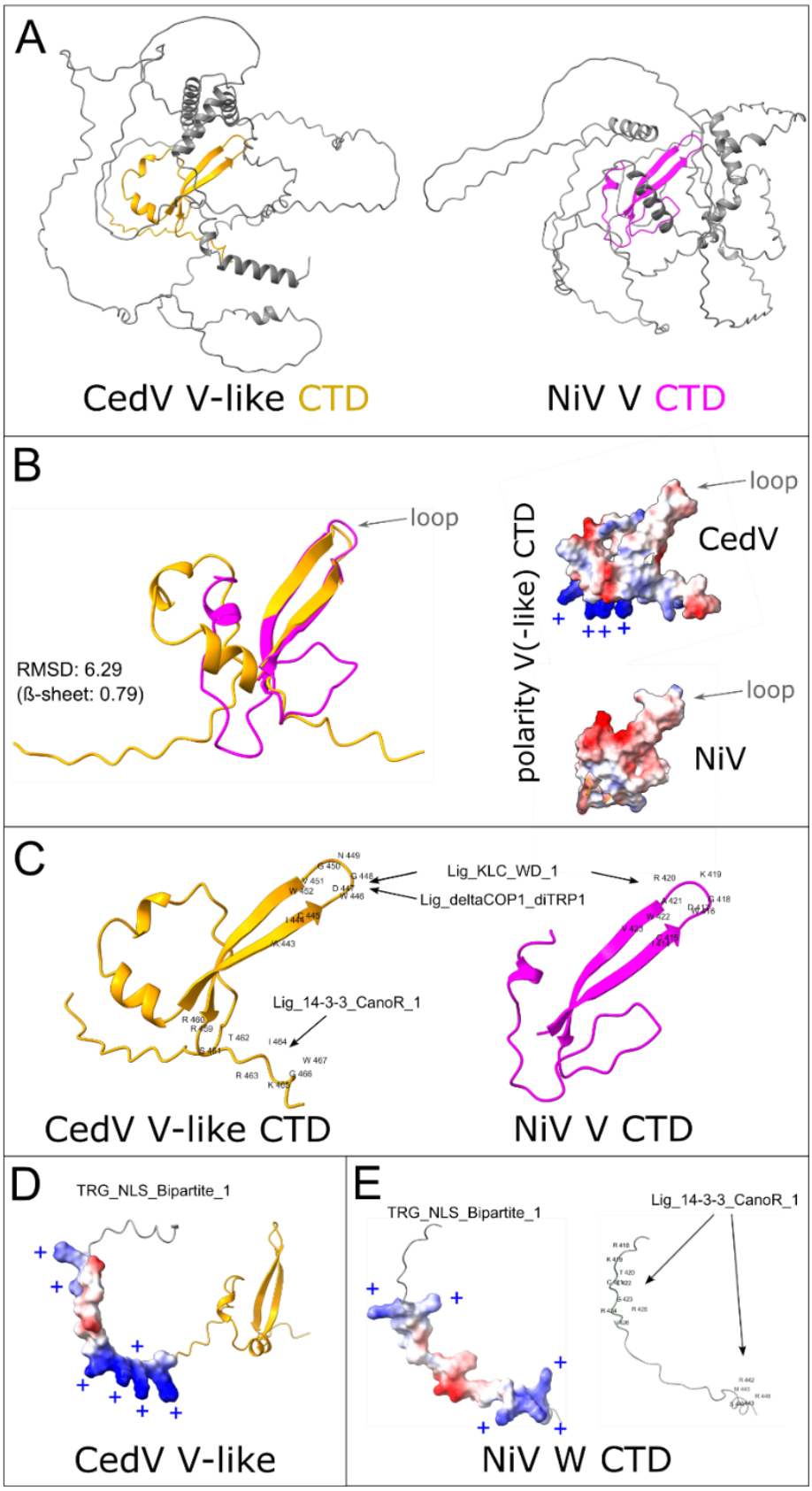
A
CedV V-like CTD
NiV V CTD
B
loop
RMSD: 6.29
(ß-sheet: 0.79)
loop
CedV
polarity V(-like) CTD
loop
NiV
C
Lig_KLC_WD_1
Lig_deltaCOP1_diTRP1
Lig_14-3-3_CanoR_1
CedV V-like CTD
NiV V CTD
D
TRG_NLS_Bipartite_1
CedV V-like
E
TRG_NLS_Bipartite_1
Lig_14-3-3_CanoR_1
NiV W CTD

860

861 **Fig.4**

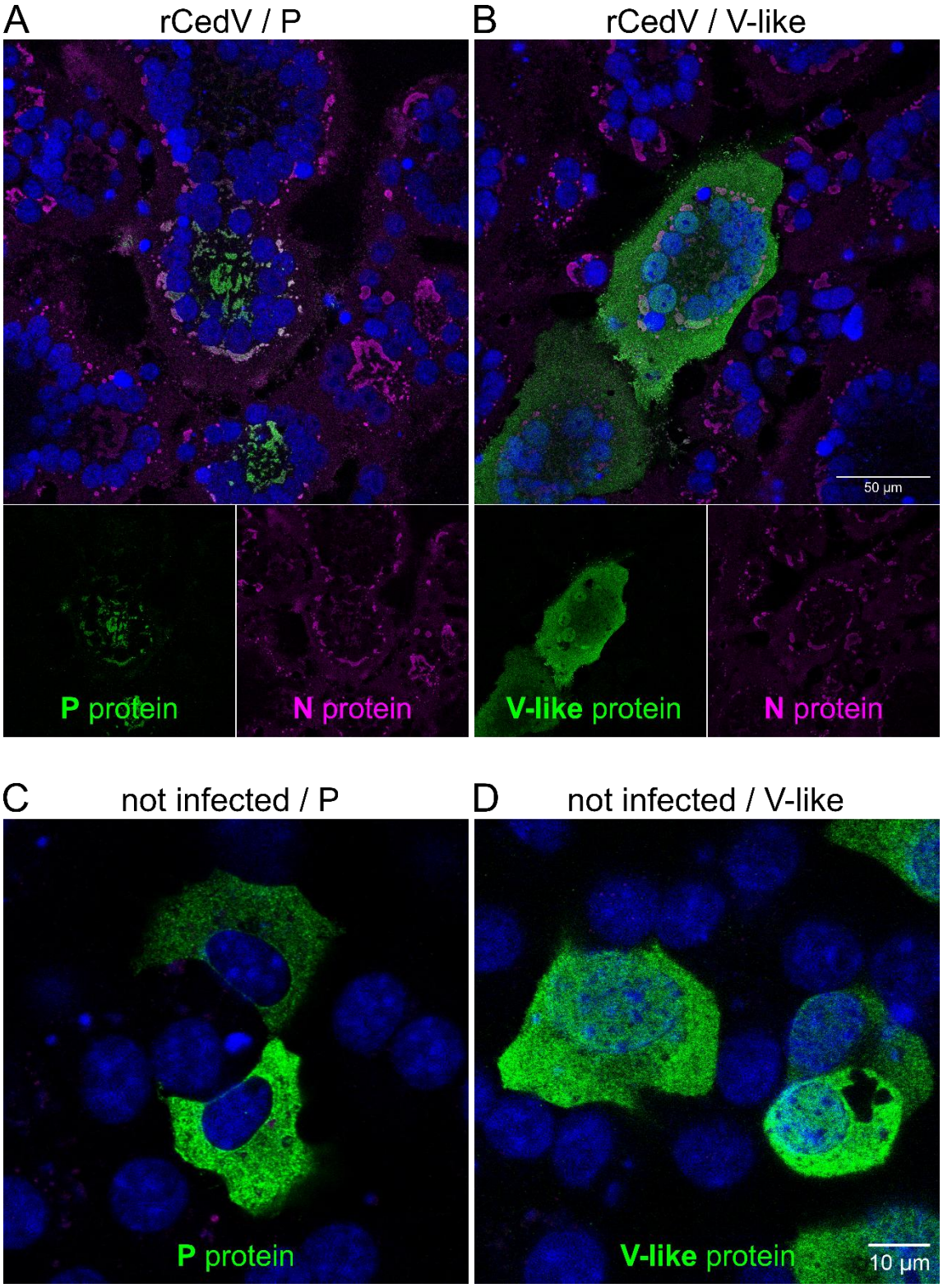
A
rCedV / P
B
rCedV / V-like
50 μm
P protein
N protein
V-like protein
N protein
C
not infected / P
D
not infected / V-like
P protein
V-like protein
10 μm

862 Fig.5

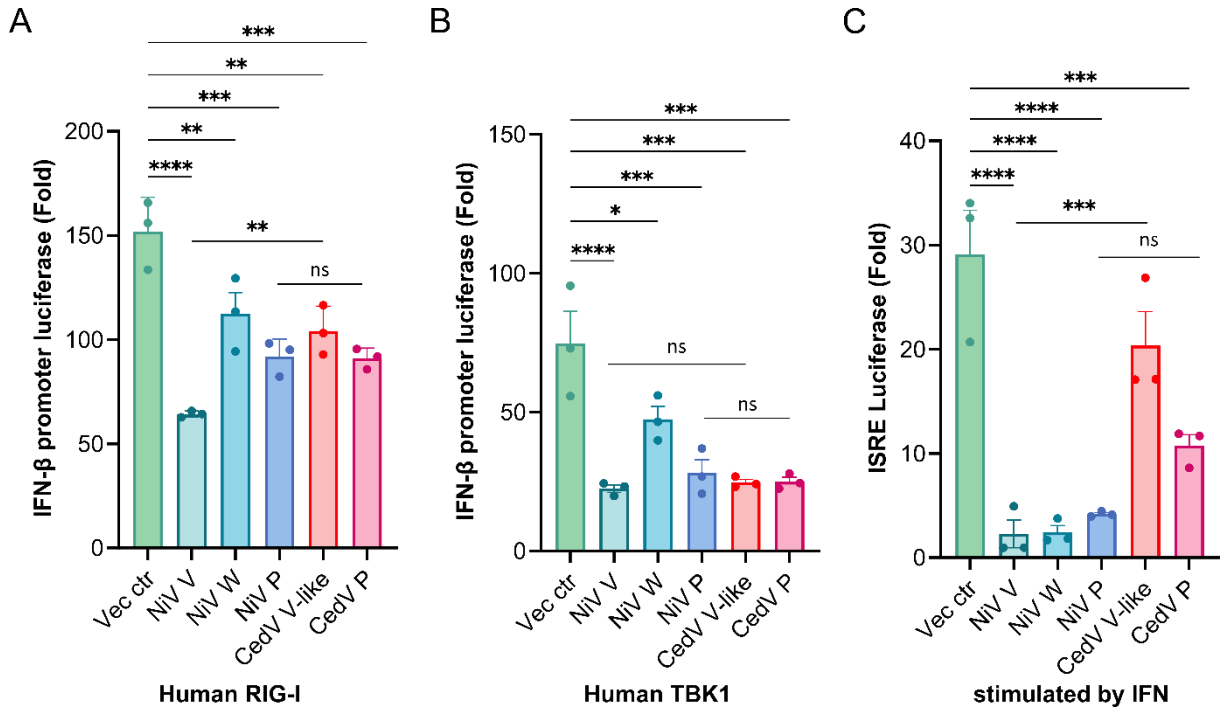
A
B
C
IFN-β promoter luciferase (Fold)
ISRE Luciferase (Fold)
Vec ctr
NiV V
NiV W
NiV P
CedV V-like
CedV P
ns
Human RIG-I
Human TBK1
stimulated by IFN

863

Fig.6

A

```
            ...AAAAAAAGAAAGGAAGGGCTAAAGGCCGCAATGCAAAAGACAAAAGA...
frame1 (P)  ..  K   K   R   K   E   G   L   K   A   A   M   Q   K   T   K   E  ..
frame3 (V-like)  ..  K   K   G   R   A   K   G   R   N   A   K   D   I   V  ..

ΔEdit-I     ...AAgAAgAGAAAGGAAGGaCTAAAGGCCGCAATGCAAAAGACAAAgGA...
frame1 (P)  ..  K   K   R   K   E   G   L   K   A   A   M   Q   K   T   K   E  ..
~~frame3 (V-like)~~

ΔEdit-II    ...AAgAAgAGAAAGGAAGGACTAAAGGCCGCAATGCAAAAGACAAAAGA...
frame1 (P)  ..  K   K   R   K   E   G   L   K   A   A   M   Q   K   T   K   E  ..
~~frame3 (V-like)~~

Stop        ...AAAAAAAGAAAGGAAGGGCTAAAGGCCGCAATGCAAAAGACtAAAGA...
frame1 (P)  ...K   K   R   K   E   G   L   K   A   A   M   Q   K   T   K   E  ..
frame3 (V-like)  ..  K   K   G   R   A   K   G   R   N   A   K   D   *
```

B

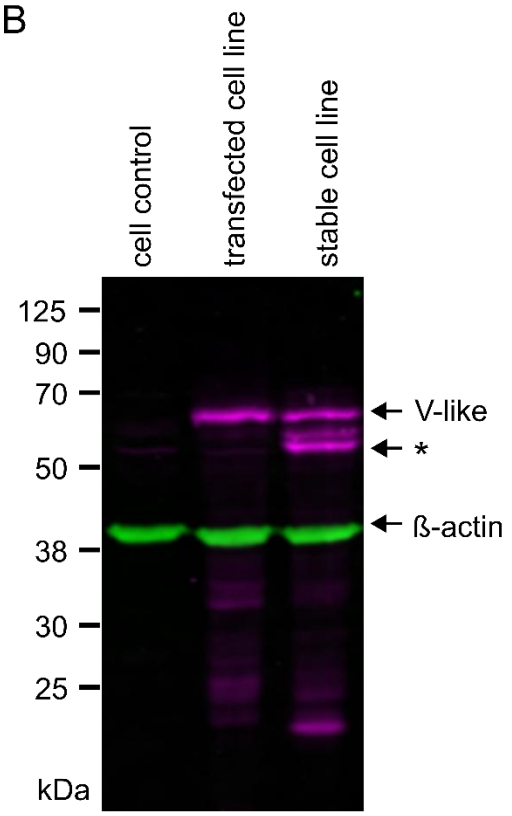

C

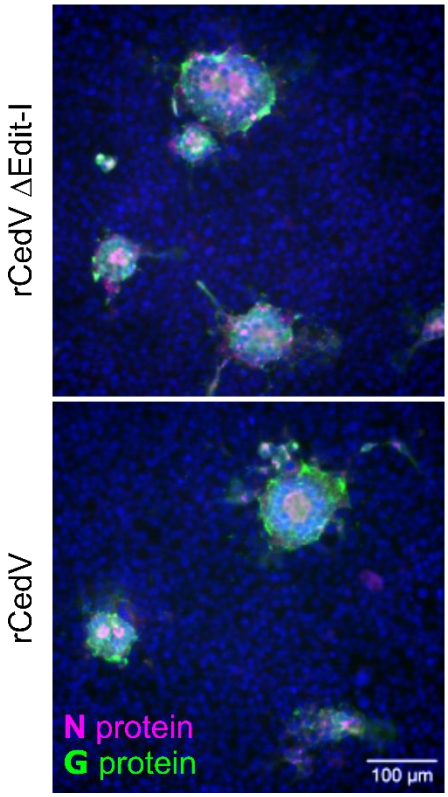

866 **Fig.7**

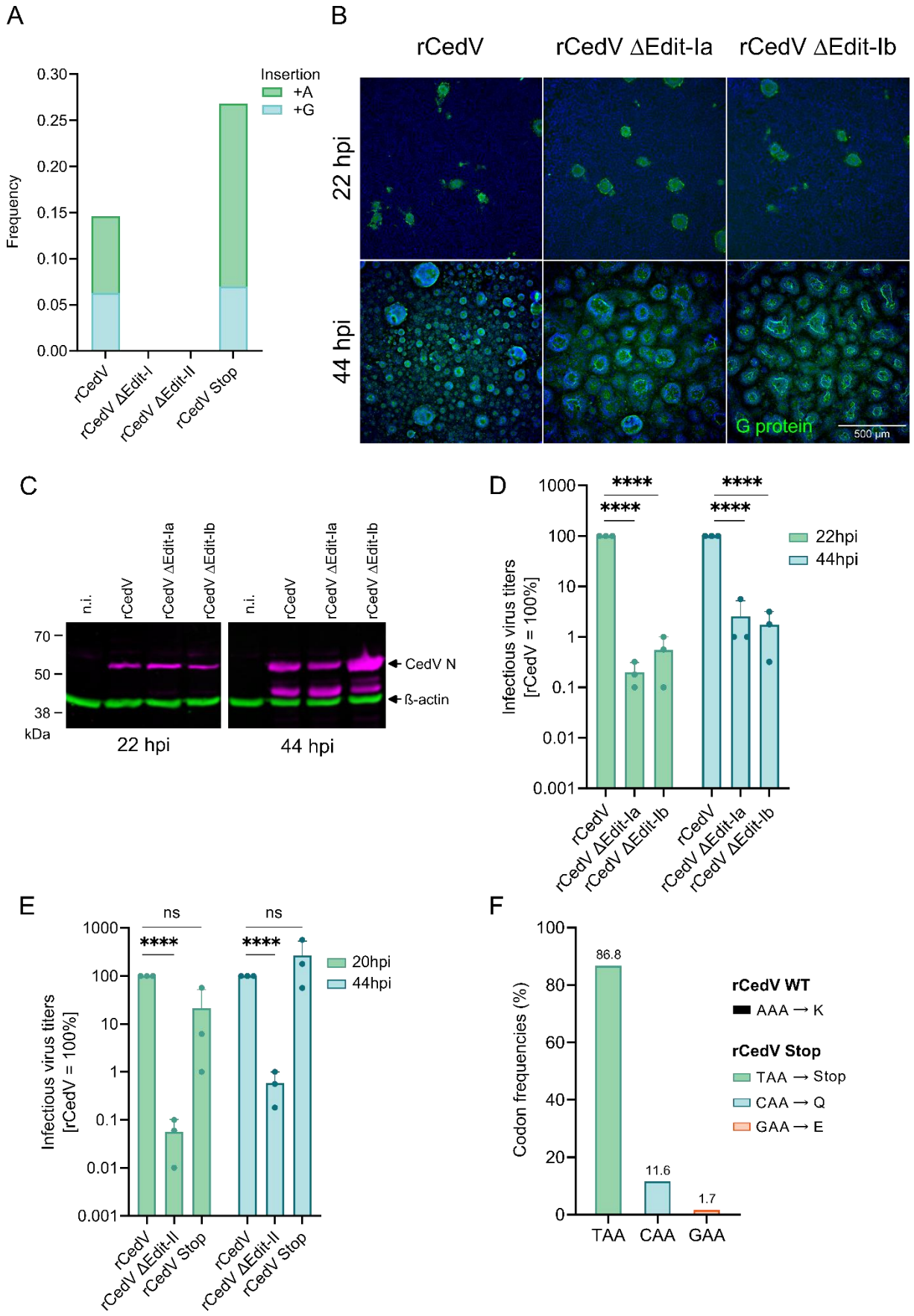
A
Insertion
+A
+G
Frequency
0.30
0.25
0.20
0.15
0.10
0.05
0.00
rCedV
rCedV ΔEdit-I
rCedV ΔEdit-II
rCedV Stop
B
rCedV
rCedV ΔEdit-Ia
rCedV ΔEdit-Ib
22 hpi
44 hpi
G protein
500 µm
C
n.i.
rCedV
rCedV ΔEdit-Ia
rCedV ΔEdit-Ib
70
50
38
kDa
CedV N
ß-actin
22 hpi
44 hpi
D
Infectious virus titers
[rCedV = 100%]
1000
100
10
1
0.1
0.01
0.001
****
22hpi
44hpi
rCedV
rCedV ΔEdit-Ia
rCedV ΔEdit-Ib
E
ns
****
20hpi
44hpi
rCedV
rCedV ΔEdit-II
rCedV Stop
F
Codon frequencies (%)
100
80
60
40
20
0
86.8
11.6
1.7
TAA
CAA
GAA
rCedV WT
AAA → K
rCedV Stop
TAA → Stop
CAA → Q
GAA → E

867

868 **Fig.8**

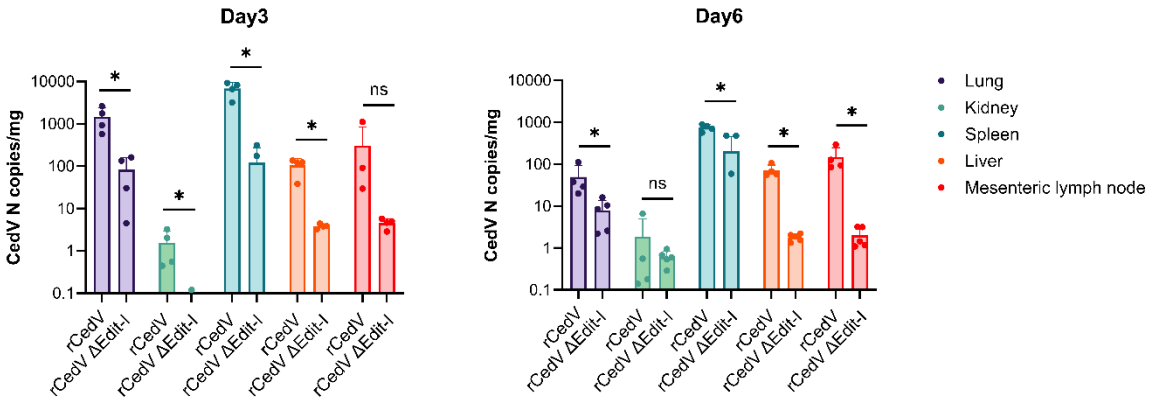
Day3
Day6
CedV N copies/mg
10000
1000
100
10
1
0.1
*
ns
rCedV
rCedV ΔEdit-I
Lung
Kidney
Spleen
Liver
Mesenteric lymph node

869